ChemComm

Cite this: *Chem. Commun.*, 2012, **48**, 8428–8430

www.rsc.org/chemcomm

COMMUNICATION

Mechanically robust 3D graphene macroassembly with high surface area†

Marcus A. Worsley,* Sergei O. Kucheyev, Harris E. Mason, Matthew D. Merrill, Brian P. Mayer, James Lewicki, Carlos A. Valdez, Matthew E. Suss, Michael Stadermann, Peter J. Pauzauskie, Joe H. Satcher Jr., Juergen Biener and Theodore F. Baumann

Received 3rd May 2012, Accepted 24th June 2012
DOI: 10.1039/c2cc33979j

We report the synthesis of a three-dimensional (3D) macroassembly of graphene sheets with electrical conductivity ($\sim 10^2$ S m^{-1}) and Young's modulus ($\sim$50 MPa) orders of magnitude higher than those previously reported, super-compressive deformation behavior ($\sim$60% failure strain), and surface areas ($>$1300 m^2 g^{-1}) approaching theoretically maximum values.

Individual graphene sheets possess a number of remarkable properties, including extremely low electrical and thermal resistivity,[1] large carrier mobility,[2] high surface area[3] and exceptional mechanical elasticity.[4] As such, graphene and graphene-based materials hold technological promise in the areas of energy storage,[5,6] electronics,[7,8] composites,[9] actuators,[10] and sensors.[11,12] Realizing the full potential of graphene in these applications, however, requires the design of bulk multifunctional architectures that retain the exceptional properties of graphene. A number of different approaches have been employed for the fabrication of 3D graphene assemblies. For example, individual graphene (or graphene oxide) sheets have been used as building blocks in the design of various macroscopic structures, including three-dimensional (3D) macroassemblies.[13–22] Typically, these 3D graphene assemblies rely on physical interactions (*i.e.*, van der Waals forces) between sheets to stabilize the network structure. As a result, these low-density ($<$100 mg cm^{-3}) 3D graphene assemblies possess Young's moduli of $\sim 10^2$ kPa and electrical conductivities of $\sim 5 \times 10^{-1}$ S m^{-1}.[14–16] Covalently bonded 3D graphene assemblies show comparatively higher electrical conductivities[13,17] and Young's moduli,[13] but the surface areas of these materials are well below 1000 m^2 g^{-1}, less than half the theoretical value for a single graphene sheet. We recently reported the synthesis of 3D graphene assemblies with high electrical conductivity.[23] Our approach involved the use of organic sol–gel chemistry to covalently cross-link graphene oxide (GO) sheets., Thermal treatment of the resulting assembly both reduced the GO to graphene and converted the sol–gel cross-links to a conductive carbon binder. These materials exhibited electrical conductivities that were significantly higher than those of physically cross-linked structures. In addition, we showed that the bulk properties of the graphene assemblies (porosity, surface area, conductivity) could be controlled through the cross-linking chemistry.[24]

In this communication, we report the fabrication of a 3D graphene macroassembly that combines high electrical conductivity, remarkable mechanical stiffness, large elastic strain, and high surface area. Instead of using sol–gel chemistry to form the assembly, these 3D graphene architectures are prepared by utilizing the chemical functionality of GO to directly cross-link the network structure. The various functional groups (*e.g.*, epoxide, hydroxide) abundant in GO sheets serve as chemical cross-linking sites for the 3D macroassembly network. Upon thermal reduction, these cross-links are transformed into conductive carbon bridges that provide structural support for the assembly, while also limiting aggregation of the individual graphene sheets. As a result, 3D graphene monoliths are obtained that exhibit mechanical stiffness and electrical conductivities orders of magnitude higher than those formed with physical cross-linking, while exhibiting super-elastic behavior and surface areas approaching the theoretical value expected for a single graphene sheet.

The 3D graphene was prepared by gelation of a GO suspension under basic conditions. The aqueous GO suspension (1–2 wt%) was prepared by ultrasonication. In a glass vial, 3 ml of the GO suspension was mixed with 500 μl concentrated NH_4OH. The vial was sealed and placed in an oven at 85 °C overnight. The resulting wet gel was washed in deionized water to purge NH_4OH followed by an exchange of water with acetone inside the pores. Supercritical CO_2 was used to dry the gels that were then converted to the final 3D graphene macroassembly by pyrolysis at 1050 °C under nitrogen. Densities of the black monoliths (Fig. S1, ESI†) were 80–100 mg cm^{-3}.

Solid-state nuclear magnetic resonance (NMR) characterization was used to gain insight into the types of functional groups in GO involved in the cross-linking process as well as to follow the reduction of GO to graphene (Fig. 1a). The GO powder contains significant epoxide and hydroxyl functionality as evidenced by numerous peaks between 50 and 75 ppm, as well as carbonyl groups (168 ppm) and sp^2 carbon (123 ppm) in its ^{13}C NMR spectrum. These peaks and assignments are consistent with the

Physical Sciences Directorate, Lawrence Livermore National Laboratory, Livermore, USA. E-mail: worsley1@llnl.gov; Fax: +1 925 422 3570; Tel: +1 925 424 4831

† Electronic supplementary information (ESI) available: Full experimental details. XRD and CV results. See DOI: 10.1039/c2cc33979j

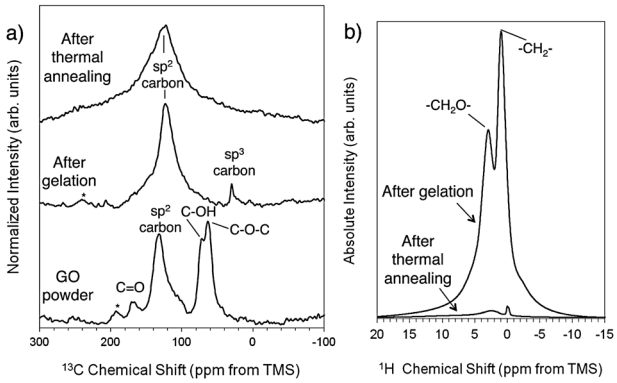

Fig. 1 ^{13}C and ^{1}H NMR spectra for GO powder, GO after initial gelation, and 3D graphene macroassembly.

existing literature.[25] After gelation, the epoxide, hydroxyl, and carbonyl peaks are virtually eliminated and an aliphatic carbon peak (26 ppm) appears. The disappearance of the large peaks between 50 and 75 ppm in the gel suggests that epoxide and hydroxyl groups are involved in the cross-linking mechanism. Conversely, the emergence of the aliphatic carbon (sp^3) peak suggests that $–CH_2–$ and/or $–CH_2O–$ are present in the gel. The $–CH_2–$ and $–CH_2O–$ moieties likely function as the cross-links that support the initial 3D GO network similar to the cross-links formed in resorcinol–formaldehyde (RF) sol–gel chemistry to form organic gels.[26,27] ^{1}H NMR spectra (Fig. 1b) for the sample after gelation also support the presence of $–CH_2–$ and $–CH_2O–$ moieties with peaks at 0.9 and 3.1 ppm. The presence of $–CH_2O–$ moieties is further supported by energy dispersive X-ray (EDX) analysis which measured 11 at% oxygen remaining in the initial aerogel. After pyrolysis, only the sp^2 carbon peak remains suggesting that the sp^3 carbon cross-links were thermally converted to conductive sp^2 carbon junctions, again analogous to the carbonization process that occurs during the pyrolysis of resorcinol–formaldehyde-based gels. The ^{1}H NMR spectrum (Fig. 1b) supports the conversion of the $–CH_2–$ and $–CH_2O–$ moieties with a virtual elimination of those peaks in the thermally treated sample. Lastly, the reduction of carbon is confirmed by oxygen content of less than 2 at%, as determined by EDX, in the final graphene assembly.

Field emission scanning electron microscopy (FE-SEM) was used to determine the microstructure of the 3D graphene. These FE-SEM images (Fig. 2) show that the 3D graphene monolith has a sheet-like microstructure similar to that reported in other graphene assemblies. In particular, the morphology resembles that of an RF-free graphene assembly reported to have a surface area in excess of 1000 $m^2\ g^{-1}$, presumably due to minimal thickness of graphene sheets.[24] Nitrogen porosimetry results for the material are consistent with the morphology revealed by FE-SEM. The nitrogen adsorption/desorption isotherm shown in Fig. 3a is Type IV, indicative of a mesoporous material. The observation of a Type 3 hysteresis loop (IUPAC classification) at high relative pressure is consistent with other 3D graphene materials, but the increased magnitude of the loop is indicative of a much larger pore volume than those reported for other graphene assemblies. The BET surface area for this graphene macroassembly is 1314 $m^2\ g^{-1}$ or roughly half of the theoretical value expected for a single graphene sheet. This extremely high surface area compared to assemblies made using sol–gel chemistry[23] suggests that layering/overlapping of sheets has been significantly reduced with the direct cross-linking approach. The reduction in layering of sheets is also consistent with an X-ray diffraction pattern that lacks a strong (002) peak at $\sim 28^\circ$ (graphite interlayer spacing) (Fig. S2, ESI†). The pore size distribution (Fig. 3b) shows that much of the pore volume (4.0 $cm^3\ g^{-1}$) lies between 3 and 10 nm, with a peak pore diameter at 6 nm.

The mechanical behavior of the 3D graphene macroassemblies was determined by flat-punch nanoindentation. Fig. 4 shows the stress *vs.* strain plot, revealing a mechanical behavior qualitatively similar to that of a carbon nanotube (CNT)-based assembly reported by Shin *et al.*[28] Loading is characterized by an initial linear-elastic region, followed by a pronounced nonlinear-elastic region. Both shape and volume of the monolith are completely restored after the load is removed. Failure is indicated by a sudden jump of the strain at a constant stress (a "pop-in" event). As previously,[28] we assign the stress and strain at the initial stage of the first pop-in event as the failure stress and failure strain, respectively. The graphene assembly has a Young's modulus of 51 ± 12 MPa, which is orders of magnitude higher than those reported for graphene assemblies.[13–16] In addition to being extraordinarily stiff, the 3D graphene monoliths exhibit super-compressive behavior with failure strains of 57 ± 21% and a complete recovery for lower strains. The failure stress is 10.4 ± 3.9 MPa. These values of failure stress and strain are comparable to those of CNT-based aerogels of the same density (100 mg cc^{-1}). These remarkable mechanical properties can be attributed to the robustness and preponderance of sp^2 carbon cross-links between graphene sheets, in addition to the excellent mechanical properties of the graphene sheets themselves.

Bulk electrical conductivity of the 3D graphene macroassembly, evaluated by the four-probe method, was measured at 100 S m^{-1}. This is consistent with carbon junctions cross-linking graphene sheets[23] and is orders of magnitude higher

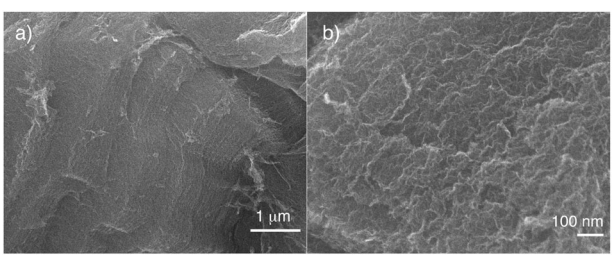

Fig. 2 FE-SEM images of the fracture surface of the 3D graphene macroassembly at (a) low and (b) high magnification.

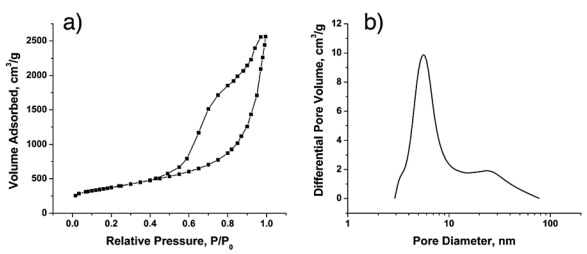

Fig. 3 (a) Nitrogen adsorption/desorption isotherm and (b) pore size distribution for the 3D graphene macroassembly.

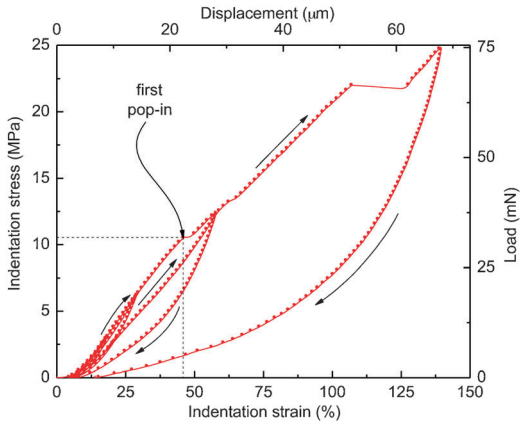

Fig. 4 Representative load-displacement (stress–strain) curve of the 3D graphene assembly (with a density of 100 mg cc^{-1}) indented with a flat punch tip with a diameter of 62 microns. Indentation was performed as a series of loading cycles with increasing maximum loads and complete unloading at the end of each load cycle.

than for graphene assemblies made *via* physical cross-links. Cyclic voltammetry (CV) was used to characterize the energy storage capabilities of the graphene assemblies in aqueous electrolyte (5 M KOH). At low scan rates, the CVs exhibit the typical rectangular shape expected for pure double-layer capacitors like conventional carbon aerogels, as well as CNT and graphene assemblies (Fig. S3, ESI†). Analysis of the CVs measured at low scan rates reveals a maximum capacitance of 165 F g^{-1} (Fig. S4a, ESI†). Remarkably, the 500 μm thick 3D graphene electrode was able to maintain greater than 50% of its maximum capacitance (89 F g^{-1}) up to 100 mV s^{-1}, indicating an exceptionally fast charge/discharge capability. The 3D graphene has a maximum energy density of 27 W h kg^{-1} and a maximum power density approaching 10 kW kg^{-1} (Fig. S4b, ESI†). Further optimization of the electrodes, such as using thinner electrodes (*e.g.* 100 μm *vs.* 500 μm thickness), and electrolyte (*e.g.* inorganic *vs.* aqueous) could push the power and energy densities to $\sim 10^2$ kW kg^{-1} and $\sim 10^2$ W h kg^{-1}, respectively. These observations illustrate the potential of 3D graphene for energy storage applications.

In summary, we have developed a 3D graphene macro-assembly material that combines high surface area, high electrical conductivity, and mechanical robustness. Our design approach utilizes the functional groups native to GO as direct cross-linking sites. These cross-links are then converted to sp^2 carbon as the GO is reduced to graphene by thermal annealing, providing strong, conductive junctions between graphene sheets. The resulting 3D graphene has large capacitance (165 F g^{-1}), high energy (27 W h kg^{-1}) and power density (10 kW kg^{-1}). In addition to energy storage applications, these 3D graphene assemblies should find application in other areas as well, including gas storage, sensors, and catalysis.

This work was performed under the auspices of the U.S. Department of Energy by Lawrence Livermore National Laboratory under Contract DE-AC52-07NA27344 and funded by LLNL's LDRD project 12-ERD-035.

Notes and references

1 X. L. Li, G. Y. Zhang, X. D. Bai, X. M. Sun, X. R. Wang, E. Wang and H. J. Dai, *Nat. Nanotechnol.*, 2008, **3**, 538–542.
2 A. K. Geim and K. S. Novoselov, *Nat. Mater.*, 2007, **6**, 183–191.
3 A. Peigney, C. Laurent, E. Flahaut, R. R. Bacsa and A. Rousset, *Carbon*, 2001, **39**, 507.
4 C. Lee, X. Wei, J. W. Kysar and J. Hone, *Science*, 2008, **321**, 385–388.
5 Y. W. Zhu, S. Murali, M. D. Stoller, K. J. Ganesh, W. W. Cai, P. J. Ferreira, A. Pirkle, R. M. Wallace, K. A. Cychosz, M. Thommes, D. Su, E. A. Stach and R. S. Ruoff, *Science*, 2011, **332**, 1537–1541.
6 M. Pumera, *Energy Environ. Sci.*, 2011, **4**, 668–674.
7 J. Biener, S. Dasgupta, L.-H. Shao, D. Wang, M. A. Worsley, A. Wittstock, J. R. I. Lee, M. M. Biener, C. Orme, S. O. Kucheyev, B. C. Wood, T. M. Willey, A. V. Hamza, J. Weissmueller, H. Hahn and T. F. Baumann, *Adv. Mater.*, 2012, DOI: 10.1002/adma.201202289.
8 F. Schwierz, *Nat. Nanotechnol.*, 2010, **5**, 487–496.
9 X. Y. Zhang, H. P. Li, X. L. Cui and Y. H. Lin, *J. Mater. Chem.*, 2010, **20**, 2801–2806.
10 L.-H. Shao, J. Biener, H.-J. Jin, M. M. Biener, T. F. Baumann and J. Weissmüller, *Adv. Funct. Mater.*, 2012, DOI: 10.1002/adfm.201200245.
11 F. Schedin, A. K. Geim, S. V. Morozov, E. W. Hill, P. Blake, M. I. Katsnelson and K. S. Novoselov, *Nat. Mater.*, 2007, **6**, 652–655.
12 H. Bai, C. Li, X. L. Wang and G. Q. Shi, *Chem. Commun.*, 2010, **46**, 2376–2378.
13 X. Zhang, Z. Sui, B. Xu, S. Yue, Y. Luo, W. Zhan and B. Liu, *J. Mater. Chem.*, 2011, **21**, 6494–6497.
14 K. X. Sheng, Y. X. Xu, C. Li and G. Q. Shi, *New Carbon Mater.*, 2011, **26**, 9–15.
15 Y. Xu, K. Sheng, C. Li and G. Shi, *ACS Nano*, 2010, **4**, 4324.
16 Z. H. Tang, S. L. Shen, J. Zhuang and X. Wang, *Angew. Chem., Int. Ed.*, 2010, **49**, 4603–4607.
17 Z. P. Chen, W. C. Ren, L. B. Gao, B. L. Liu, S. F. Pei and H. M. Cheng, *Nat. Mater.*, 2011, **10**, 424–428.
18 Z. Sui, X. Zhang, Y. Lei and Y. Luo, *Carbon*, 2011, **49**, 4314–4321.
19 W. Chen and L. Yan, *Nanoscale*, 2011, **3**, 3132–3137.
20 F. Liu and T. S. Seo, *Adv. Funct. Mater.*, 2010, **20**, 1930–1936.
21 Z. Niu, J. Chen, H. H. Hng, J. Ma and X. Chen, *Adv. Mater.*, 2012, DOI: 10.1002/adma.201200197.
22 S. Yin, Z. Niu and X. Chen, *Small*, 2012, DOI: 10.1002/smll.201102614.
23 M. A. Worsley, P. J. Pauzauskie, T. Y. Olson, J. Biener, J. H. Satcher and T. F. Baumann, *J. Am. Chem. Soc.*, 2010, **132**, 14067–14069.
24 M. A. Worsley, T. Y. Olson, J. R. I. Lee, T. M. Willey, M. H. Nielsen, S. K. Roberts, P. J. Pauzauskie, J. Biener, J. H. Satcher and T. F. Baumann, *J. Phys. Chem. Lett.*, 2011, **2**, 921–925.
25 W. Gao, L. B. Alemany, L. J. Ci and P. M. Ajayan, *Nat. Chem.*, 2009, **1**, 403–408.
26 S. A. Al-Muhtaseb and J. A. Ritter, *Adv. Mater.*, 2003, **15**, 101–114.
27 R. W. Pekala and F. M. Kong, *Abstracts of Papers of the American Chemical Society*, 1989, 197, 113-POLY.
28 S. J. Shin, S. O. Kucheyev, M. A. Worsley and A. V. Hamza, *Carbon*, 2012, DOI: 10.1016/j.carbon.2012.06.044.

